Acta Astronautica 172 (2020) 33–46

Contents lists available at ScienceDirect

Acta Astronautica

journal homepage: www.elsevier.com/locate/actaastro

Design and demonstration of micro-scale vacuum cathode arc thruster with inductive energy storage circuit

Yueh-Heng Li[a,*], Jun-You Pan[a], Georg Herdrich[b]

[a] Department of Aeronautics and Astronautics, National Cheng Kung University, Tainan, 701, Taiwan
[b] Institute of Space Systems (IRS), University of Stuttgart, Stuttgart, 70569, Germany

ARTICLE INFO

Keywords:
Electric propulsion
Vacuum cathode arc thruster
Plasma
Exhaust velocity
Single impulse
Specific impulse

ABSTRACT

This study focused on the development of a vacuum cathode arc thruster (VAT), particularly on its design, manufacturing process, and demonstration. Characteristically, the proposed thruster does not require any additional propellant feeding system as the cathode electrode is simultaneously used as a propellant. In the ignition system, tiny spots are coated on the cathode surface to induce plasma flow. Such a setup has the advantages of simplicity, low price, small size, and low weight and is suitable for microsatellites. Moreover, a "trigger-less" method with an inductor storage power system was used for generating the pulsed plasma. This discharge method can significantly reduce input power. Thrust is mainly caused by high exhaust velocities of metal ions in the plasma flow, making ion density, ion velocity, and ion charge influential parameters. A battery was used instead of a power supply system to reduce the energy consumption of the entire VAT processing unit. The energy required for a single pulse was estimated to be 0.266 J, by measuring the change between the discharge current and the voltage. The ion current was measured using an ion detector and was 3.55 A, and the ion velocity was 23150 m/s. In the theoretical analysis, the VAT prototype proposed in this study achieved a single impulse of 4.31 μNs, a specific impulse of 1571 s, and a thrust efficiency of approximately 12.5%.

1. Introduction

There are two primary systems in the space propulsion technology—chemical propulsion (CP) and the electric propulsion (EP). In chemical propulsion, thrust is produced by severe chemical reactions and considerable exothermicity. Thrust in EP is produced by the reaction force generated when plasma is expelled by means of propellant acceleration. For EP the propellant's enthalpy is driven by external electric energy. Compared with the conventional CP, EP has a higher specific impulse, but lower thrust. If the specific impulse (I_{sp}) is higher, the fuel consumption is comparably much lower. Correspondingly, CP is inevitable to offset Earth's gravity. However, once the rocket successfully enters space, the EP is more useful than chemical propulsion in the long-hauling operation. Plasma comprises a group of electrons, ions, radicals, and neutrals (if the plasma is not fully ionized). As the mass of an electron smaller than that of an ion, the effect of an electron can be neglected during the propulsion process. In general, the EP mechanism can be categorized into three types based on the ion acceleration mechanism as electrothermal, electrostatic, and electromagnetic [1]. Moreover, it is not practical to scale existing EP systems such as ion and Hall thrusters to the range of 1–10 W. The unavoidable flow controls and plumbing and the overhead mass of the propellant storage tank reduce the overall efficiency of ion thrusters at the aforementioned power levels. Therefore, these types of propulsion systems are not appropriate for the use in cube satellites.

To enable microsatellites to achieve capabilities such as attitude control, position maintenance, and orbital transformation, new types of micro- and nano-thrusters should be developed to provide a wide range of impulse bits with the corresponding values spanning from nano-Newton-seconds to micro-Newton-seconds. Thus, pulsed plasma thrusters (PPTs) [39,40] and vacuum cathode arc thrusters (VATs) [41] have proved to be good candidates for fulfilling many missions that require impulse bits approximately in the range of nano-Newton-seconds to milli-Newton-seconds [2–4]. Both types of thrusters can be easily miniaturized with maintaining their power based on the mission requirements. Therefore, they are suitable for microsatellites or CubeSat propulsion systems. Although PPTs can provide impulse bits approximately in the range of micro-Newton-seconds to milli-Newton-seconds, the use of Teflon material causes low fuel efficiency and the requirement of a peak operating voltage of approximately 2 kV. Essentially, the overall efficiency of a very small PPT is approximate 12% [5]. To reduce the restriction of miniaturization in power system, a vacuum

* Corresponding author. Department of Aeronautics and Astronautics, National Cheng Kung Univ., Tainan, 701, Taiwan.
E-mail address: yueheng@mail.ncku.edu.tw (Y.-H. Li).

https://doi.org/10.1016/j.actaastro.2020.03.012
Received 12 May 2019; Received in revised form 2 March 2020; Accepted 9 March 2020
Available online 13 March 2020

cathode arc thruster (VAT) was used in this study. An inductive energy storage device [6] in combination with trigger-less ignition methods [7] was implemented. This configuration presents many benefits, such as a decrease in the size of a thruster, a decrease in the operating voltage required, and no need of an igniter. Most importantly, the VAT is also suitable for use in microsatellites or a CubeSat and can provide impulse bits approximately in the range of nano-Newton-seconds to micro-Newton-seconds.

The vacuum arc plasma source is a good candidate as a thruster because it has the capability of using any conductive metal or alloy as its fuel [7,8], low power consumption, variable thrust capability, and low system mass. The cathode material generates metal plasma, neutral gas, and macroparticles by a vacuum arc discharge from a cathode spot [9,10]. The metal plasma plume moves outward to achieve velocity in the range of 1–3 $\times$ 10^4 m/s for a wide range of materials, that is, from carbon to tungsten. Moreover, the VAT usually operates in the pulse mode with energy in the range of 1–100 W. These characteristics revealed that the VAT is a potential candidate for micro- and nano-propulsion. In summary, the VAT was selected and developed as the main development thruster of a microsatellite in this study.

The earliest VAT literature was published by Dethlefsen in 1968 [11] and Gilmour and Lockwood in 1972 [12]. They tested a variety of cathode materials and successfully used the axial magnetic field to focus the ejected plasma jet. Subsequently, it discovered that when the VAT operates in the pulse mode, high power densities are required within the arc while maintaining low average power and small system size. The study of VATs was restarted from 1998 and continued till 2005 by the collaboration between Alameda Applied Sciences Corporation (AASC), NASA/Caltech Jet Propulsion Laboratory, and the Lawrence Berkeley National Laboratory (LBNL) [13–15]. During that time, some major technological breakthroughs were achieved, such as the development of an inductive energy storage device [6], the combination of the inductive energy storage device and the trigger-less ignition method [16], and the use of a compact magnetic coil for collimating and accelerating plasma [12,17]. In addition, Neumann et al. [18] demonstrated a Mg-fuelled centre-triggered pulsed cathodic arc thruster and it explored higher current centre-triggered pulsed arcs with greater impulse bits, specific impulses and thrust-to-power ratios. In recent years, many scholars have begun to think about how to increase the performance and lifetime of a VAT [19,20]. The applied magnetic field has significantly improved the efficiency and lifetime of a thruster [18,21]. Other study results revealed that the thrust and plasma distribution can be improved by changing the shape of the cathode.

Currently, VAT development focuses on CubeSat propulsion subsystems. This includes studies conducted by the Kyushu Institute of Technology development on HORYU nanosatellites [19], the University of Federal Armed Forces in Germany on the UWE-4 nanosatellite [22], and the US Air Force BRICSat-P CubeSat [23] and George Washington University's participation in the PhoneSat Project at NASA Ames Research Center [24]. This shows that an increasing number of countries are dedicating themselves to the development of VATs. As VATs are still in their preliminary stage of development, some theoretical models of VATs have been published [13,25,26]. In the past twenty years, Statom used some vacuum arc empirical data and a basic energy balance to estimate the ratio of kinetic energy and electrical energy and attempted to understand the phenomenon of plasma [26]. Sekerak and Polk et al. have developed a semiempirical model to more accurately determine the performance of VAT for a wide range of cathode materials [13,25].

In principal, any electrically conductive solid metal, compound, or alloy can be used as a propellant for the VAT due to their high density and high electrical and thermal conductivities. Researchers typically select metals that have high melting points, high boiling points, and relatively low electron work functions to fulfill the basic requirements that are derived from a cathode operation for a VAT. Some experimental results revealed the performance of periodic metal elements when they are applied to a VAT [27]. However, it is still a challenge to determine the most suitable metal. Different metal materials have different thermophysical and electrical properties. These characteristics can even affect the performance of the thruster. However, many factors influence these characteristics, such as the state of the cathode surface, the presence of particles, and the discharge condition of the vacuum arc. Although the VAT is still in the preliminary research stage, this study used copper and aluminum as cathode materials after considering the accessibility and affordability of metal materials. Moreover, studies have indicated that some carbon- and graphite-based materials are effective propellants for the VAT [28,29]. Carbon has high-temperature resistance and sublimes rather than melting, and its resistance decreases with increase in temperature. Graphite-based materials present better erosion rate results and higher amount of ions compared with the carbon-based materials. Therefore, researchers believed that carbon and graphite materials have the potential for application in VATs [28,29]. To apply the propulsion system to microsatellites, the miniaturization of electric propulsion and its auxiliary units are important without jeopardizing their function and thrust performance. Accordingly, this study developed micro function generators and micropulse discharge circuit design integrated with VAT system. Moreover, we tried to use a battery instead of a power supply to generate a pulse discharge. Eventually, experiments have confirmed that this set of VAT prototypes exhibits high stability and repeatability during operation.

2. Experimental setup

2.1. Vacuum chamber and pump system

All tests in this study were conducted in a stainless-steel cylindrical vacuum chamber with a size of 50 $\times$ 60 cm^2 (diameter $\times$ length). The vacuum chamber has several flanges for internal and external circuit connections and signals acquisition. The pump system comprises an oil-free scroll dry pump (PTS06003 UNIV, Agilent Technologies Inc., Santa Clara, CA, United States), a turbo molecular pump (HIPace 80, Pfeiffer Vacuum GmbH, Asslar, Germany), and a water cooling system. Among them, the dry pump was used first to decrease the chamber pressure to less than 0.073 hPa. Then, the turbo molecular pump was used to achieve medium vacuum (MV, 0.1–10^{-3} hPa) and high vacuum (HV, 10^{-3} to 10^{-7} hPa) conditions for realizing a vacuum environment. The turbo-molecular pump speed can be accelerated from zero to tens of thousands of revolutions. High speed is accompanied by a high value of friction. Thus, it must be ensured that when the turbo molecular pump was switched on, the chamber pressure was less than 0.073 hPa and the water cooling system should be cooled. Otherwise, damage can be caused by the turbine blades. Conversely, a stainless-steel spring tube was connected between the vacuum chamber and the pump system to prevent the transmission of vibration between the pump system and the vacuum chamber during the pump operation. Pressure readings were obtained using a vacuum gauge (Penningvac PTR 90 N, Leybold GmbH, Cologne, Germany), which allows a complete measurement range of 1.33 $\times$ 10^{-9} hPa to atmospheric pressure by using a single transmitter. The entire vacuum system used an automatic control system to achieve the switching purpose and used a display panel for immediate monitoring and operation. The atmospheric pressure of approximately five hPa was introduced to push the vacuum valve to achieve the pumping capacity of the entire vacuum system. This vacuum system can reach 10^{-7} hPa. However, all tests were performed at 10^{-5} hPa to simulate the low-orbit vacuum conditions of the Earth (LEO). The vacuum system configuration is displayed in Fig. 1. Fig. 2 displays a schematic of the overall vacuum system.

2.2. Pulse discharge circuit

In this study, the prototype of the inductive energy storage circuit [30] was tested and applied to the VAT prototype. This prototype

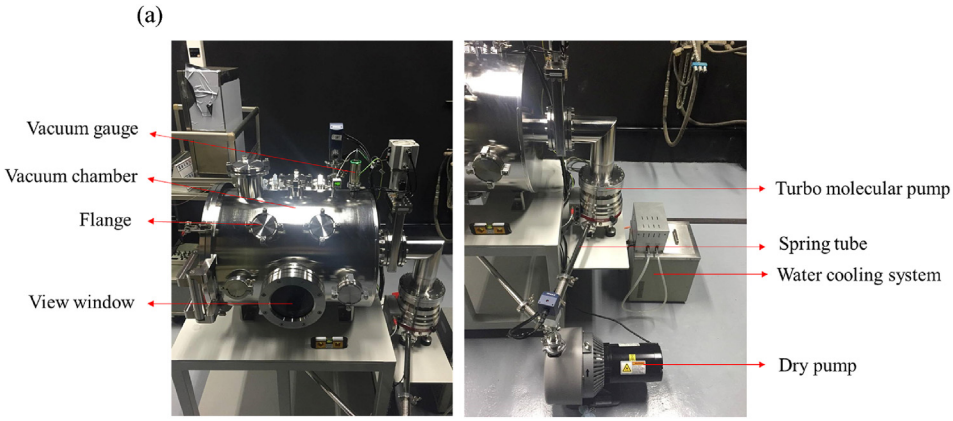

Fig. 1. Vacuum system configuration.

successfully achieves the purpose of pulse discharge. Based on the circuit design, we tried to design a preliminary pulse discharge circuit in this study. The schematic is illustrated in Fig. 3.

A power supply that provides an adjustable DC voltage input in the range of 20–60 V was used in the circuit. The function generator adjusts the desired discharge frequency and charging time to control the Insulated Gate Bipolar Transistor (IGBT) switch. When the function generator provides a TTL square wave signal, the inductive component can store energy in the form of a magnetic field. When the TTL signal reduces to 0 V, the IGBT forms an open circuit. Based on Lenz's and Faraday's laws, the inductor induces a high voltage (700–1000 V) to maintain the current for resisting changes in the current (di/dt). The induced voltage causes VAT breakdown and induces a discharge current from the circuit, thus causing the VAT to discharge plasma for generating thrust.

Moreover, the VAT ejects plasma to generate thrust. During the discharging process, the arc regulates its own voltage to maintain the discharge. With time, when the discharge current is insufficient to maintain the arc (this current is also known as chopping current), the arc will be extinguished and complete discharge. At this point, the IGBT was switched on again, and the inductor was recharged to prepare for the next pulse discharge. In this circuit, the IGBT was the key in the entire circuit and was responsible for controlling the main charging and discharging process. Therefore, the power specification of the IGBT limits discharge power. Table 1 summarizes the performance of this discharge circuit.

2.3. Cathode erosion rate measurement

In the operation principle, a VAT uses the cathode as a fuel for generating thrust. Therefore, the erosion rate of the cathode (fuel) is an important indicator in this study. The most commonly used measure of erosion rate was the cathode weight-loss method [31,32]. Other methods included measuring the ion erosion rate and imaging and calculating the lost volume of the cathode surface. Compared with these methods, the cathode weight-loss method is the most direct and convenient method. This method can reliably measure the weight loss of a cathode and provide a reference value for subsequent analysis of the results. By estimating the mass loss of the cathode before and after the experiment and the total amount of the pulse accumulated during the discharge, the cathodic erosion rate can be expressed as follows:

$$\mathrm{Er} = \frac{\Delta m}{Q_{total}}, \tag{1}$$

where Er is the cathode loss rate in μg/C, Δm is the weight loss of ions, and Q is the total charge of the pulse discharge. The total pulse discharge amount can be obtained using the following formula

$$Q_{total} = \bar{I}\, t_{pulse}\, f\, t_{operation}, \tag{2}$$

where $\bar{I}$ is the average discharge current releasing from the inductor, t_{pulse} is the pulse discharge time, f is the frequency, and $t_{operation}$ is the total test time. With the aforementioned information, the mass flow rate of a VAT can be obtained using the cathode loss rate, pulse arc current, and VAT discharge duty cycle

$$\dot{m} = Er\, \bar{I}\, t_{pulse}\, f, \tag{3}$$

where $t_{pulse}f$ is the duty cycle (the ratio of the working time to the total time in one cycle).

2.4. Langmuir probe

The Langmuir probe is the simplest and most commonly used method for plasma measurement [33,34]. By inserting a metal probe into the plasma group to be tested and setting an appropriate scanning

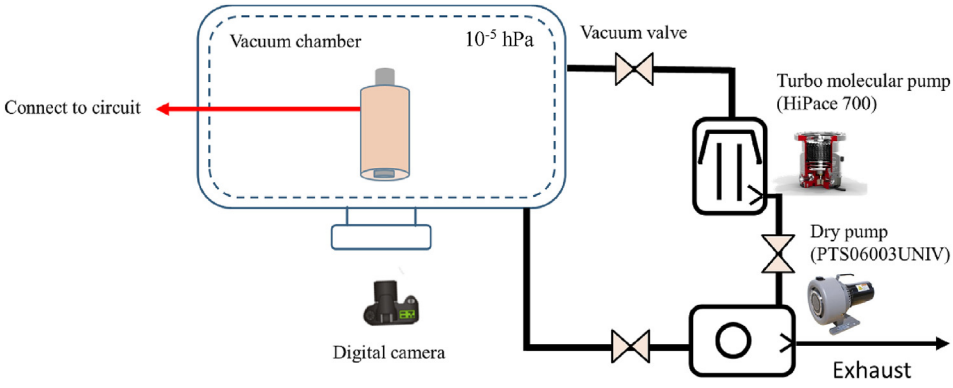

Fig. 2. Overall experimental configuration concept diagram of the vacuum system.

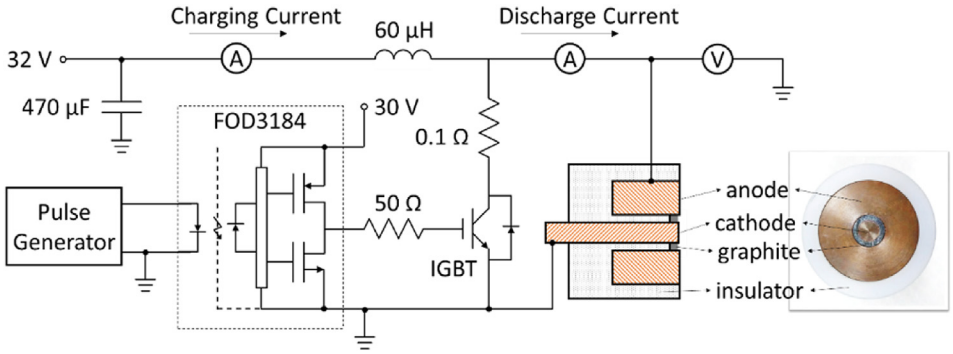

Fig. 3. Pulse discharge circuit.

Table 1
Performance of the pulse discharge circuit.

Parameter	Min	Max
Power supply voltage (V)	20	60
Discharge voltage (V)	30	40
Discharge current (A)	30	100
Pulse frequency (Hz)	1	20
Pulse length (μs)	60	300
Discharge power (W)	0.33	6.64

voltage, the difference between the plasma potential and the probe potential attracts electrons or ions in the plasma to generate a net current. Based on this measured net current, the plasma density and temperature could be estimated. Although this interventional measurement can cause some errors, it could still provide a reference value for the initially established propulsion system. Langmuir probes are of three types—single, double, and triple probes. The single and double probes obtain a net current based on a given scanning voltage. This characteristic is advantageous for steady-state systems, such as plasma measurement in flames. The pulse discharge system developed in this study has a high dependence on the time scale. Therefore, it was necessary to use triple probes with the time resolution because a bias voltage was provided instead of a scanning voltage [30].

2.5. Voltage and current measurement

The thruster discharge process can be divided into two phases—the front-end circuit energy-processing unit and the back-end plasma plume ejection unit. Therefore, before measuring the plasma plume parameters, it is necessary to know how much energy the circuit provides to the thruster. Energy can be obtained by integrating the voltage and current curves during charging and discharging as follows:

$$E = \int IVdt = \sum IV\Delta t, \tag{4}$$

where E is the energy in Joule, I is the current in Ampère, and Δt is the time difference of each data.

A high-voltage probe (the induced voltage generated by the inductor is 700–1000 V) and a magnetic induction current meter were used to measure the voltage and current. The experimental configuration is displayed in Fig. 4.

The magnetic induction current meter was placed in the loop of the power supply and the IGBT to measure how much current is charged into the inductor. Then, the magnetic induction current meter and the high voltage probe were placed in the loop of the IGBT and the VAT to measure the discharge current and the discharge voltage. Finally, by analyzing the data acquired by the oscilloscope, it is possible to estimate the conversion efficiency of charging and discharging the circuit energy-processing unit and to determine how much energy the circuit actually outputs to the VAT.

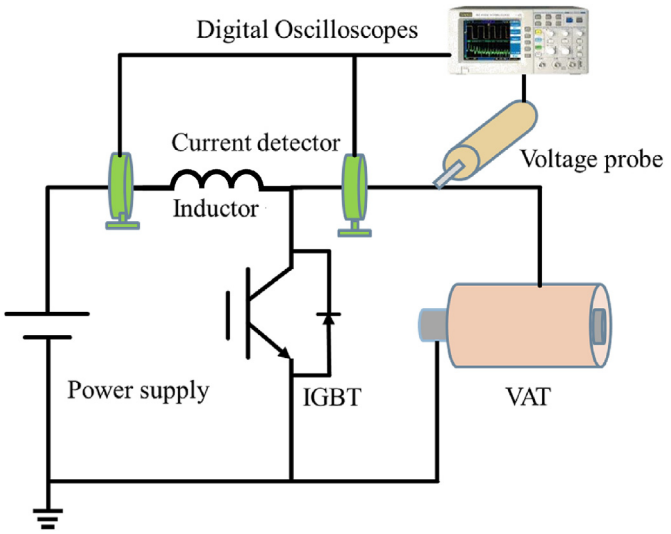

Fig. 4. Diagram of the experimental configuration.

2.6. Ion current measurement

Regarding plasma plume measurement, this study used the most direct and simple method to measure ion current and ion velocity. Two circular grids were placed in front of the thruster (the grid must cover the entire plasma plume). Given the proper bias to the grids, it is possible to exclude electrons (or ions) and only allow ions (or electrons) to pass through the grids. By using this method, the total ion current (or total electron current) flowing between the two grids was measured. For a given bias estimation, the energy conservation formula is as follows

$$\frac{1}{2}\mathrm{m}\vec{V}^2 = \mathrm{eV}, \tag{5}$$

where m is the mass of a single electron or ion; $\vec{V}$ is the exit velocity of electrons or ions; eV is the energy of the grid where e is the basic charge of 1.6×10^{-19} C and V is the voltage. Based on this formula, it is assumed that all ions have a positive charge, the mass of one aluminum ion is 2.16×10^{-26} kg, and the aluminum ion velocity in the reference is 15400 m/s [17]. The bias voltage required to exclude aluminum ions is 16 V. As the literature pertaining to a VAT did not present a detailed discussion of the electron energy [17], this study uses this grid measurement method to determine the different bias voltages to observe the optimal bias value of the excluded electrons. The total ion current passing between the two grids was measured. The actual configuration is shown in Fig. 5.

In the experimental configuration, to prevent the bias potential of the grids from interacting with the electrode potential of the thruster, the grids were placed approximately 10 mm away from the thruster for

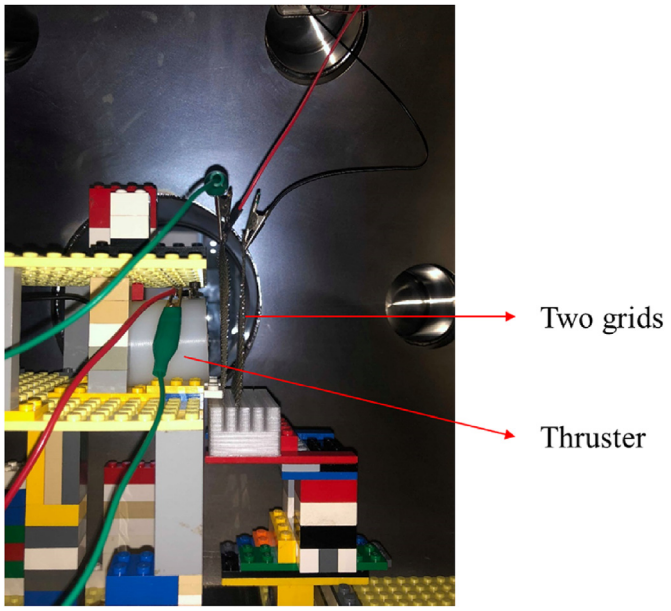

Fig. 5. Configuration of the two electric grids.

measurement. The distance between the two grids was 5 mm. This section describes the final design of the overall propulsion system, including the thruster design and the pulsed discharge circuit design. To apply the propulsion system to microsatellites, this study developed micro function generators and micropulse discharge circuit design, among others. Moreover, we attempted to use a battery instead of a power supply to generate a pulse discharge. Experiments have confirmed that this set of VAT prototypes exhibits high stability and repeatability during operation. In the future, this prototype can be used to further optimize the VAT geometry and discharge circuits to improve performance.

3. Concept and design of the VAT system

3.1. VAT prototype design

The VAT comprises a cathode, an anode, and an insulator. For the preliminary design, this study uses the design of a coaxial VAT with a solid cathod rod inserted into the insulating tube and surrounded by the anode. This proposed design was compared with other existing VAT designs. The symmetrical nature of the coaxial VAT design simplifies the analysis of the subsequent plasma plume. Under the premise of microsatellites and experiments, the design of a VAT should be as simple, cheap, convenient, and fast as possible. In the actual design, the size of the thruster is limited because the ceramic tube (alumina) is not easy to process. In this study, a ceramic tube was selected from those available in the market, and the scale of the cathode rod with the inner diameter was determined. As the anode has thermal deposition problems, and the vacuum arc is not entirely understood, the anode design in this study was based on the design of Lun [35]. The final thruster design was obtained after conducting some revision and evaluation and is presented in Fig. 6.

A commercial ceramic tube (alumina) with an inner diameter of 6 mm and an outer diameter of 10 mm was selected as the insulator. Therefore, a metal rod with a diameter of 6 mm was selected as the cathode. To facilitate installation, the metal rod was inserted into the ceramic tube and fit tightly. Moreover, the anode was equipped with a metal ring with an outer diameter of 30 mm and an inner diameter of approximately 10 mm; the anode surrounded the ceramic tube. The VAT housing was fabricated using ultra-high molecular weight polyethylene (UHMWPE), which has high insulation, easy processing, and low cost. During the experiment, the VAT was allowed to be installed conveniently and quickly, and the VAT components can be easily replaced. The anode and the VAT housing fabricated using UHMWPE were fixed with plastic screws to avoid sliding during the experiment. Regarding connecting circuits, the cathode was simply connected using an alligator clip, and a metal screw was used to connect the anode. The cathode and the insulator are not set in the same plane as the anode and are recessed from the anode end to prevent contamination of the anode surface due to the products generated because of vacuum arc discharge. This exerts a weak influence on thrust generation. By analyzing the overall VAT design and discharge evaluation, the cathode and insulator were recessed by 0.5 mm from the anode end. This setting does not significantly affect the thrust generation and simultaneously reduces the pollution caused by the anode. The entire thruster is a cylinder of approximately 40 mm (diameter) × 50 mm (length) and weighs approximately 120 g.

3.2. Pulse discharge circuit design

Based on the energy storage circuit developed by Schein et al. [30], we tried to design a preliminary pulse discharge circuit and improve the circuit. Finally, the inductor storage circuit suitable for this experiment was designed and displayed in Fig. 7.

This circuit design contains a few additional components. In addition to providing higher power, capacitors also have the ability to prevent any damage to the power supply. The diode was used to prevent the back-end voltage or current peak from flowing back because the backward flow causes damage to the power supply. The optocoupler driver was used to convert a transistor–transistor logic (TTL) square-wave signal into a voltage signal (± 15 V) to drive the IGBT (semiconductor switch). The operation of the inductive energy storage circuit could be divided into three stages:

(1) First stage:

In this stage, the IGBT gate voltage is set to −15 V. This ensures that the IGBT is in the open state. In this circuit, both the IGBT component and the VAT are open; thus, the power supply only supplies voltage to the capacitor for charging. As presented in Fig. 8, during the charging process of the capacitor, the formula of the capacitance-voltage value with time (t) can be expressed as follows based on Kirchhoff's voltage law

$$V_c(t) = V_p\left(1 - e^{-\frac{t}{RC}}\right), \tag{6}$$

where V_C is the capacitor voltage, V_P is the voltage supplied by the power supply, R is the resistance in the circuit, and C is the capacitance. Based on this formula, the capacitance-voltage is a function of the circuit resistance and the elapsed time. During the charging process of the capacitor, the current expression based on the Kirchhoff's current law is as follows

$$I(t) = \frac{V_p}{R}e^{-\frac{t}{RC}}. \tag{7}$$

This formula reveals that the charging current decreases with time. When the capacitor attains the preset target voltage value, the first stage of the capacitor charging process is completed.

(2) Second stage:

In this stage, the IGBT gate voltage is set to +15 V. This causes the IGBT to enter the conduction mode. At this point, the current supplied by the power supply and the capacitor flows through the path of the inductor and the IGBT. As the power provided by the capacitor is greater than that supplied by the power supply, it can be assumed that all the energy stored in the inductor was from the capacitor, as

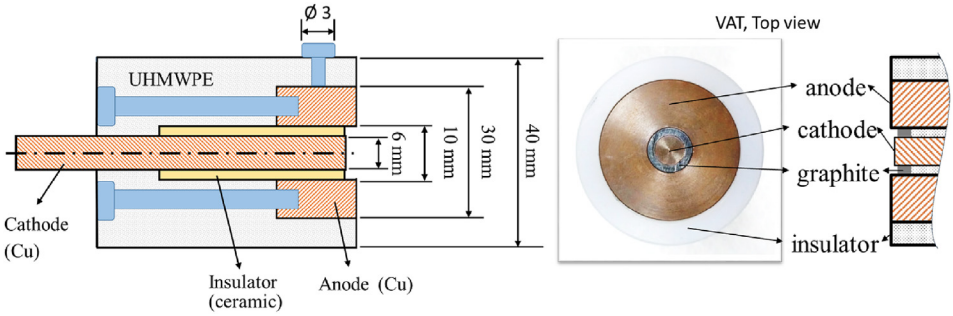

Fig. 6. Coaxial VAT final design.

illustrated in Fig. 9. During the charging process of the inductor, the change in current with time can be expressed as follows

$$I(t) = \frac{V_p}{R}\left(1 - e^{-\frac{Rt}{L}}\right), \tag{8}$$

where V_P is the voltage supplied by the power supply, R is the resistance in the circuit, and L is the inductance value. The inductor charging stage is considered completed when the current flowing through the inductor attains the maximum value.

(3) Third stage:

In this stage, the IGBT gate is set to −15 V. This turns the IGBT into the open mode so that no current flows through the IGBT. To resist the current transformation, the inductor generates a high voltage to maintain this current (V(t) = L di/dt). The voltage peak is applied to the VAT, and the carbon layer between the cathode and the anode is subjected to a small current generated by the voltage to evaporate and slightly ignite, thereby releasing the energy stored in the inductor to form a vacuum arc discharge. When the discharge is completed, it implies that the discharge stage of this inductor is completed. When the inductor is discharged, the power supply simultaneously charges the capacitor to prepare for the next discharge, as shown in Fig. 10.

Under ideal conditions, it is assumed that the energy stored in the capacitor is completely transformed into the energy stored in the inductor. To maximize the energy processing efficiency of the circuit, the capacitance and inductance values must be simply evaluated and matched, and the energy stored in the capacitor can be estimated using the following formula:

$$E_c = \frac{1}{2}CV^2. \tag{9}$$

Similarly, the energy stored in the inductor can be estimated using the following formula:

$$E_L = \frac{1}{2}LI^2. \tag{10}$$

Based on the law of conservation of energy ($E_C = E_L$), the foregoing two equations can be rewritten as follows:

$$L = C\frac{V^2}{I^2}. \tag{11}$$

Based on this formula, the voltage supplied by the power supply is 30 V, the capacitance value is 1200 μF, and the peak current can be as high as 50 A. The inductance value should be 432 μH. In this study, the inductance is 440 μH.

The results of the study revealed that during the experiment, the inductor was charged under the RLC circuit and exhibited a Gaussian distribution. As presented in Fig. 11, there exists an optimum charging time that maximizes the current flowing through the inductor. If this charging time is exceeded, the current flowing through the inductor decreases, thus causing the energy stored in the inductor be lower. This behavior is because the energy stored in the inductor is from the capacitor. When the energy of the capacitor is released, the energy stored in the inductor attains the maximum value. Therefore, the width of the TTL square-wave signal can be controlled to determine the time during which the IGBT was switched on, thereby adjusting the charging time of the inductor.

3.3. Microfunction generator design

This study attempts to replace the signal generator with a simple circuit to facilitate subsequent circuit integration and miniaturization of the overall VAT system. By using a silicon oscillator (LTC6991, Analog Device Inc., Massachusetts, USA) to achieve this goal by conducting a series of resistor and capacitor matching, the required width and

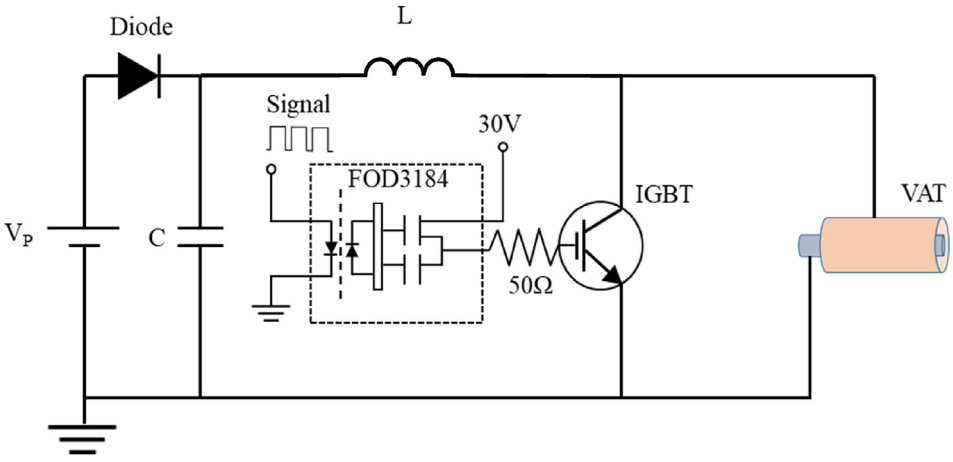

Fig. 7. The final design of the inductive energy storage circuit.

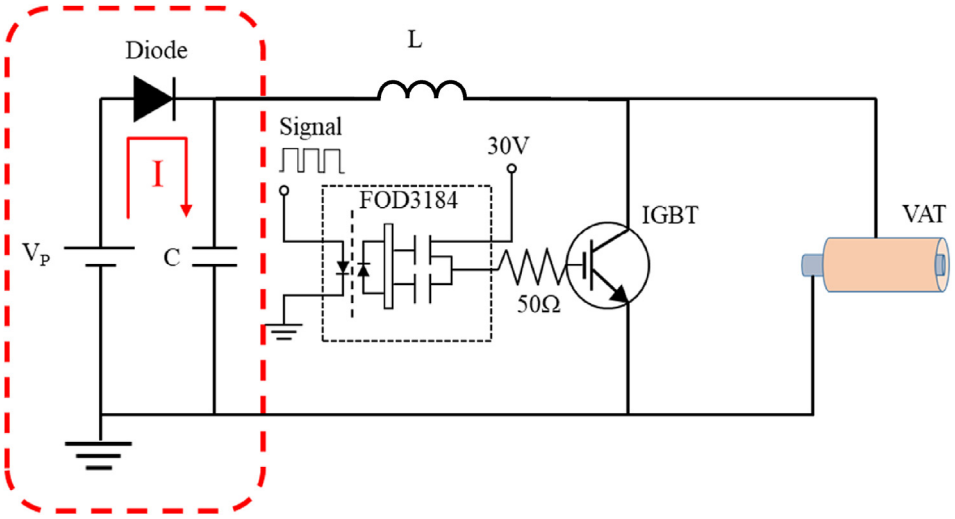

Fig. 8. Schematic of the first stage of the capacitor charging circuit.

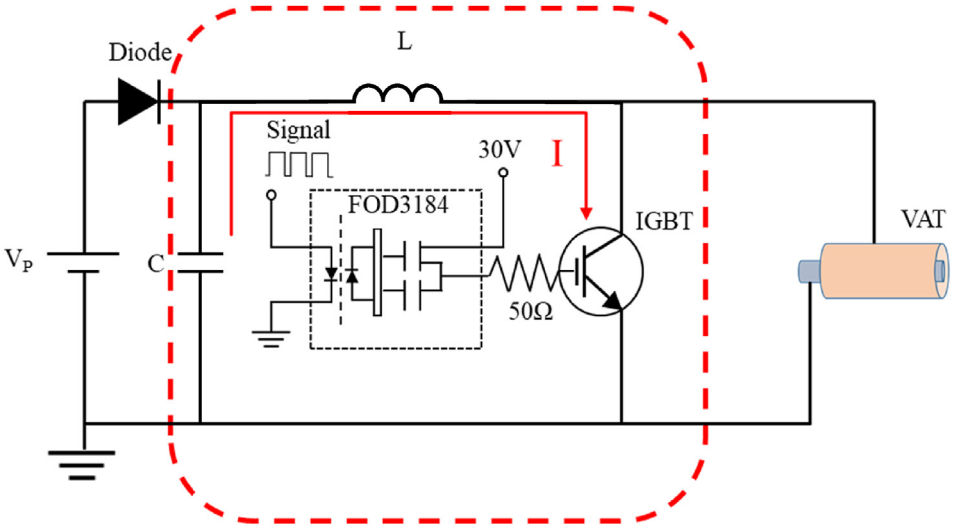

Fig. 9. Schematic of the second stage of the inductor charging circuit.

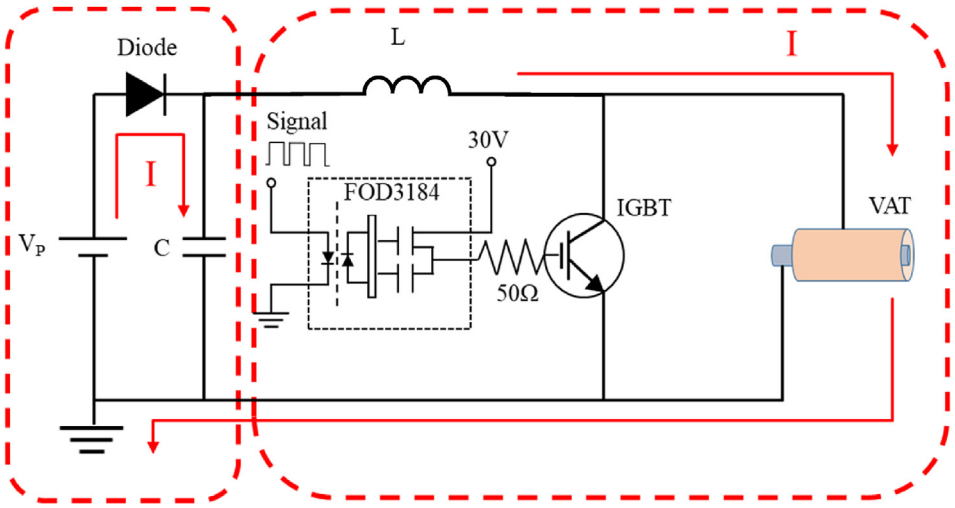

Fig. 10. Schematic of the third stage of the inductor discharge circuit (simultaneous with the first stage).

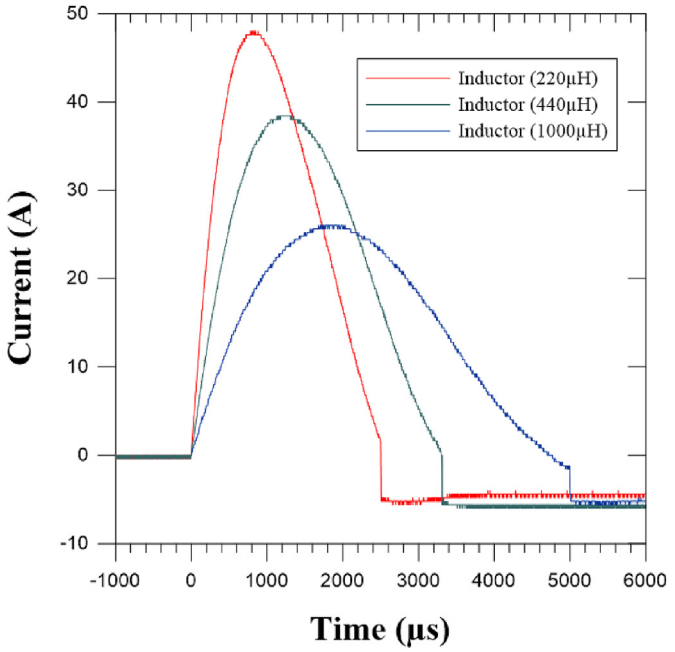

Fig. 11. Inductive charging curves of 220 μH with 800 μs, 440 μH with 1200 μs, and 1000 μH with 1800 μs).

frequency of the square wave can be designed. Fig. 12 presents the microfunction generator circuit, and a few simple steps are provided to illustrate the design process and present the specifications of the electronic components.

(1) Step 1: Determine square wave period, POL, N_{DIV}, R_1, and R_2

Select the required square wave period t_{out} based on Table 2, and select the high potential signal POL = 0, which is a positive square-wave signal.

The following formula was used to determine the divider ratio N_{DIV}

$$\frac{t_{out}}{16.384ms} \leq N_{DIV} \leq \frac{t_{out}}{1.024ms} \tag{12}$$

As N_{DIV} is obtained in the form of a range, if a value is repeated in the comparison table, the smaller value should be selected. The corresponding R_1 and R_2 should be found after determining N_{DIV} to match the voltage (voltage divider rule).

(2) Step 2: Determine the frequency-setting resistor R_{SET} and the width of the square wave t_{pulse}

The following formula was used to determine R_{SET}:

$$R_{SET} = \frac{50K\Omega}{1.024ms}\frac{t_{out}}{N_{DIV}} \tag{13}$$

Then, the following formula was used to determine R_{pw}:

$$t_{pulse} = -R_{pw}\, C_{pw} \ln\left(1 - \frac{V_{RST(RISING)}}{V^+}\right) \tag{14}$$

$V_{RST(RISING)}$ can be expressed as follows:

$$V_{RST(RISING)} = 0.55^+ + 185\text{mV} \tag{15}$$

Here, t_{pulse}, input voltage V^+, V_{RST}, and the other parameters are known. A C_{pw} value of 470 pF was recommended by this product; thus, R_{pw} can be obtained.

(3) Step 3: Output test

After the preceding steps, this study successfully miniaturized the function generator with a condition of 1 Hz and a square-wave width of 800 μs. The oscilloscope was used to actually test the results, as shown in Fig. 13.

To easily integrate the VAT system into the microsatellites in the future, this study attempted to replace the power supply with a battery, as shown in Fig. 14.

The power supply was replaced with a 4-V lithium-ion battery (NCR18650B) and a DC-DC converter (TP-3020, Twintex Instrument Ltd., Taiwan). Unfortunately, after several successful discharges, the DC-DC converter became hot and stopped discharging. This was because, in the circuit design, the discharge current required by the thruster is greater than the upper limit of the power of the DC-DC converter. Thus, the converter was idling and became hot. However, this method proves that the overall circuit system can be miniaturized. When the DC-DC converter matching the discharge current of the thruster was successfully designed, the circuit could be reproduced again.

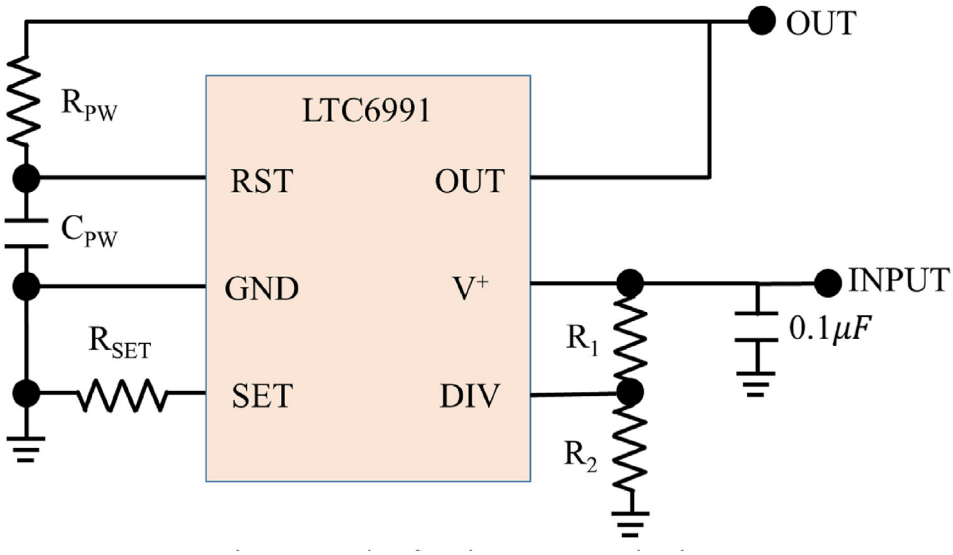

Fig. 12. Microfunction generator circuit.

Table 2
Period and resistance matching table.

DIVCODE	PDL	N_{DIV}	Recommended t_{out} (s)	R_1 (kΩ)	R_2 (kΩ)	V_{DIV}/V^+
0	0	1	1.024×10^{-3} to 16.384×10^{-3}	Open	Short	≤ 0.03125 ± 0.015
1	0	8	8.912×10^{-3} to 0.131	976	102	0.09375 ± 0.015
2	0	64	65.5×10^{-3} to 1.05	976	182	0.15625 ± 0.015
3	0	512	0.524 to 8.39	1000	280	0.21875 ± 0.015
4	0	4096	4.19 to 67.1	1000	392	0.28125 ± 0.015
5	0	32768	33.6 to 537	1000	523	0.34375 ± 0.015
6	0	262144	268 to 4295	1000	681	0.40625 ± 0.015
7	0	2097152	2174 to 34360	1000	887	0.46875 ± 0.015
8	1	2097152	2174 to 34360	887	1000	0.53125 ± 0.015
9	1	262144	268 to 4295	681	1000	0.59375 ± 0.015
10	1	32768	33.6 to 537	523	1000	0.65625 ± 0.015
11	1	4096	4.19 to 67.1	392	1000	0.71875 ± 0.015
12	1	512	0.524 to 8.39	280	1000	0.78125 ± 0.015
13	1	64	65.5×10^{-3} to 1.05	182	976	0.84375 ± 0.015
14	1	8	8.912×10^{-3} to 0.131	102	976	0.90625 ± 0.015
15	1	1	1.024×10^{-3} to 16.384×10^{-3}	Short	Open	≥ 0.96875 ± 0.015

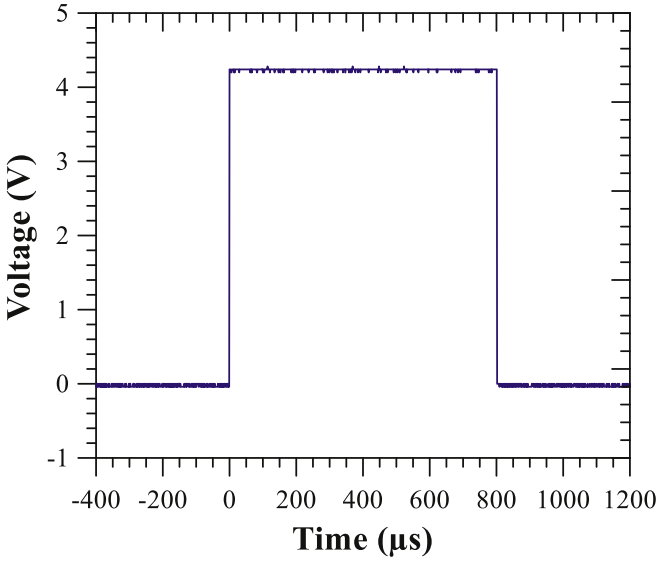

Fig. 13. Microfunction generator output square wave (1 Hz, 800 μs).

4. VAT demonstration

A VAT prototype was independently developed in this study. After conducting a series of evaluations and designs, the construction of the entire VAT system was finally completed. Then, the system was successfully ignited to confirm its feasibility and stability.

4.1. Vacuum arc discharge process

In the plasma propulsion classification, a VAT is classified as an electrothermal-type device. By using a tiny arc caused by an instantaneous high voltage, the carbon layer was slightly exploded and evaporated, and a conductive vapor was formed in vacuum to induce a vacuum arc. During the discharge process, the energy of the vacuum arc adjusted itself to the position that is the most favorable for discharge. Thus, a cathode spot was formed and was usually in the micrometer scale. As the energy is concentrated in such a small place, the cathode spots have a high energy density, which is consistent with the conditions of the thermionic emission mechanism. These thermionic ions accelerate outwardly through the partial pressure gradient to generate thrust. Thus, the surface of the cathode was found to be erosive; thus, the next cathode spot was formed at another position that is favorable for discharge. In the actual VAT process test, it was found that the vacuum arc was randomly formed on the surface of the cathode. This implies that the formation of cathode spots is random, and the actual discharge is displayed in Fig. 15.

Fig. 15 presents a close-up image of the VAT prototype discharge at a vacuum pressure of 10^{-5} hPa. The figure presents that the plasma plume produced by the erosion of aluminum metal is biased toward light blue, and the light blue plasma plume is diffused out from the surface of the VAT, which also contains some large particles of incandescence. Conversely, under the same environmental conditions, the plasma plume produced by copper metal is biased toward pink, as presented in Fig. 16. This behavior is because different metal atoms have different ionization energies and thus correspond to plasma plumes of different colors.

To understand the entire discharge process in a better manner, a

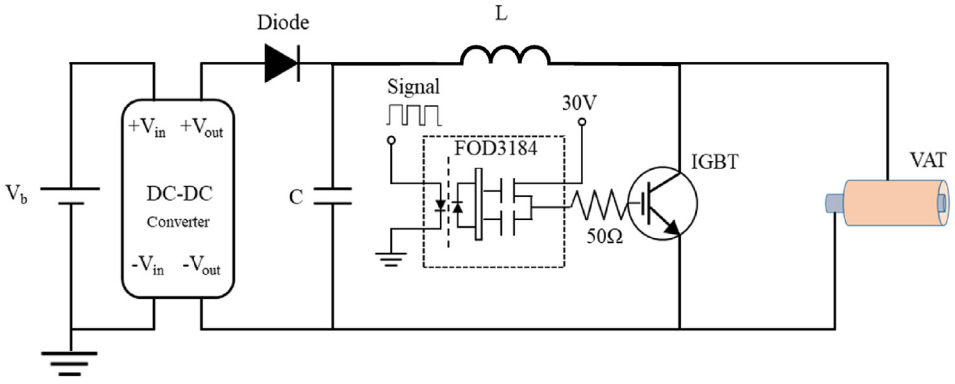

Fig. 14. The battery used to replace the power supply.

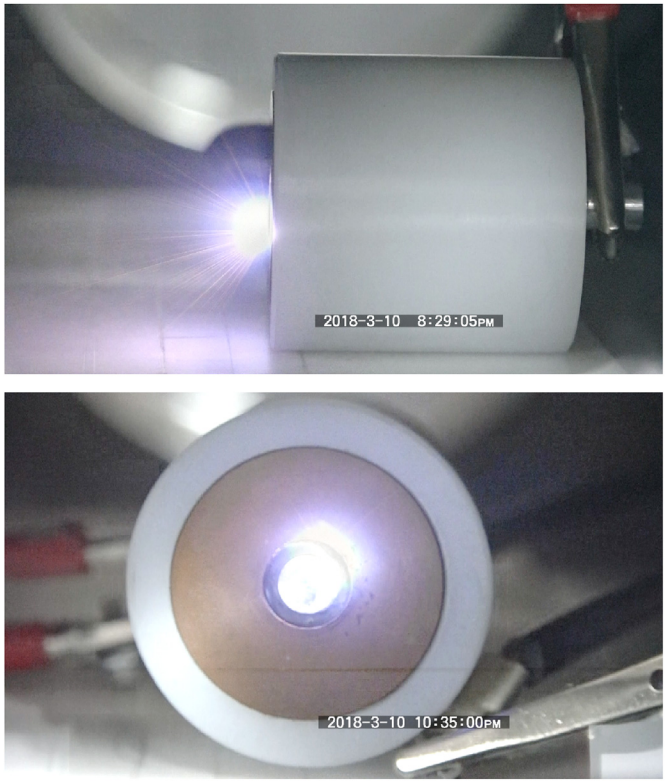

Fig. 15. Discharging of a VAT with an Al cathode: side view (top) and front view (bottom).

high-speed camera (FASTCAM SA5, Photron Limited) was used to record the discharge process of the VAT. FASTCAM SA5 can capture images at up to 3,00,000 frames per second (fps), but the resolution is very low (128 × 16 pixels). After actual adjustment, the minimum resolution required is 512 × 288 pixels to observe the entire thruster surface. Thus, for the camera, 50,000 fps (resolution: 512 × 288 pixels) and a Nikon AIS 85 mm lens were used to capture images. When images are taken at 50,000 fps, it is implied that an image is taken after every 20 μs. Moreover, when the VAT is in the range of 300–400 μs for each discharge, 15–20 images can be captured. As presented in Fig. 17, the initial stage of the vacuum arc formation could be clearly observed at 20 μs. However, it was found that the formation of a vacuum arc produces a tiny spark between the cathode and the anode despite the asymmetrical and stochastic occurrence on the interface between cathode and graphene layer. Then, the two sparks form a vacuum arc, which is similar to the tip discharge concept. The generation of the vacuum arc due to the fading can be clearly observed in the image, which implies that the energy stored in the inductor is released from this moment to the end. At 200 μs, the electrons that are less energetic in the plasma plume are attracted by the anode potential, thus causing the electrons to bombard the anode surface.

4.2. Circuit charging and discharging process

To understand the energy conversion during VAT discharge, a high-voltage probe and current meter were used to measure the charging and discharging of the inductive energy storage circuit. Eq. (10) presents that the higher the inductance value, the higher is the amount of energy stored in the inductor. Three different inductors with inductance values of 220 μH, 440 μH, and 1 mH were tested. The inductor was charged and discharged under the condition that the power supply provides 30 V, and the result is shown in Fig. 18.

The time required for the large inductor to reach current saturation was longer and the current is smaller. However, large-capacity

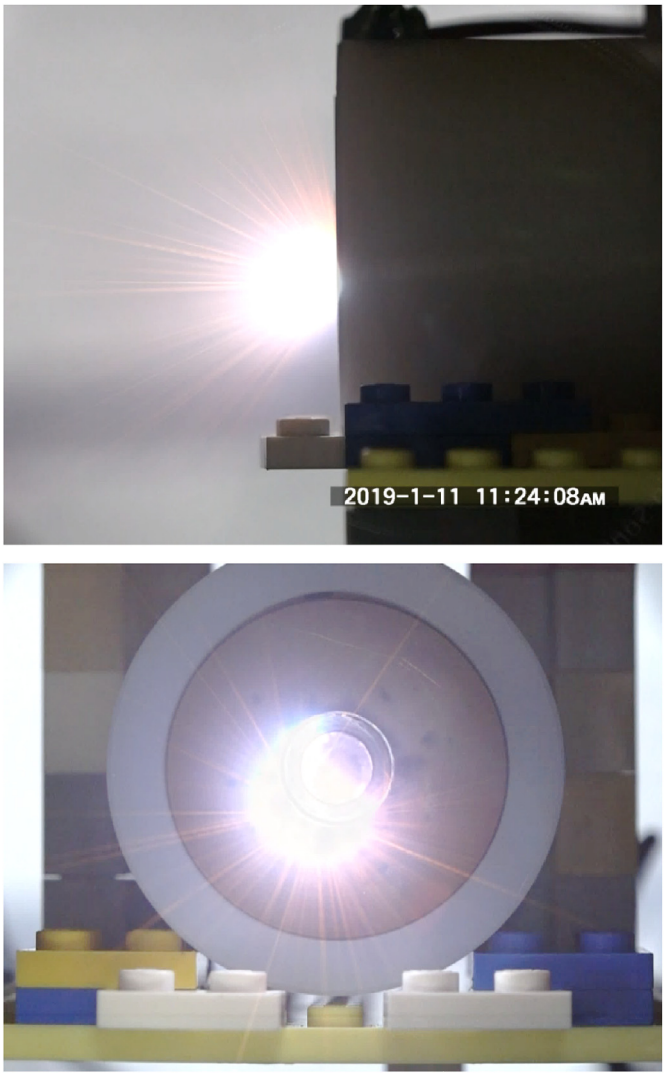

Fig. 16. Discharging of a VAT with a Cu cathode: side view (top) and front view (bottom).

inductors can store higher amounts of energy. Through the ratio of the output energy of the inductor to the input energy, the energy conversion efficiencies of the inductor were estimated to be 87.6%, 94.3%, and 81.6% for the inductance values of 220 μH, 440 μH, and 1 mH, respectively. The inductor with the inductance value of 440 μH is the most suitable for 1200 μF. As presented in Eqs. (4)–(6), based on the capacitance and inductance values, the value of 440 μH is the most appropriate. If the discharge frequency varies from 1 to 20 Hz, the energy attains a value in the range of 0.33–6.64 W, which is in line with the microsatellite application power range of 1–10 W.

4.3. Plasma plume detection

Due to the asymmetrical and stochastic occurrence of a plasma jet on VCAT, the probe measurement system is not appropriate to engage for plasma measurement, but the grid measurement system. As described, two grids were placed at the VAT outlet, and a positive electric field was applied to accelerate the ions through the grid. This positive electric field excludes electrons, thereby measuring the total ion flux in the plasma plume. The conceptual diagram is displayed in Fig. 19. In addition, the ion charge state number was assumed one.

To ensure that the bias between the grids does not affect the VAT discharge, the grid was placed 50 mm from the exit end of the VAT, and

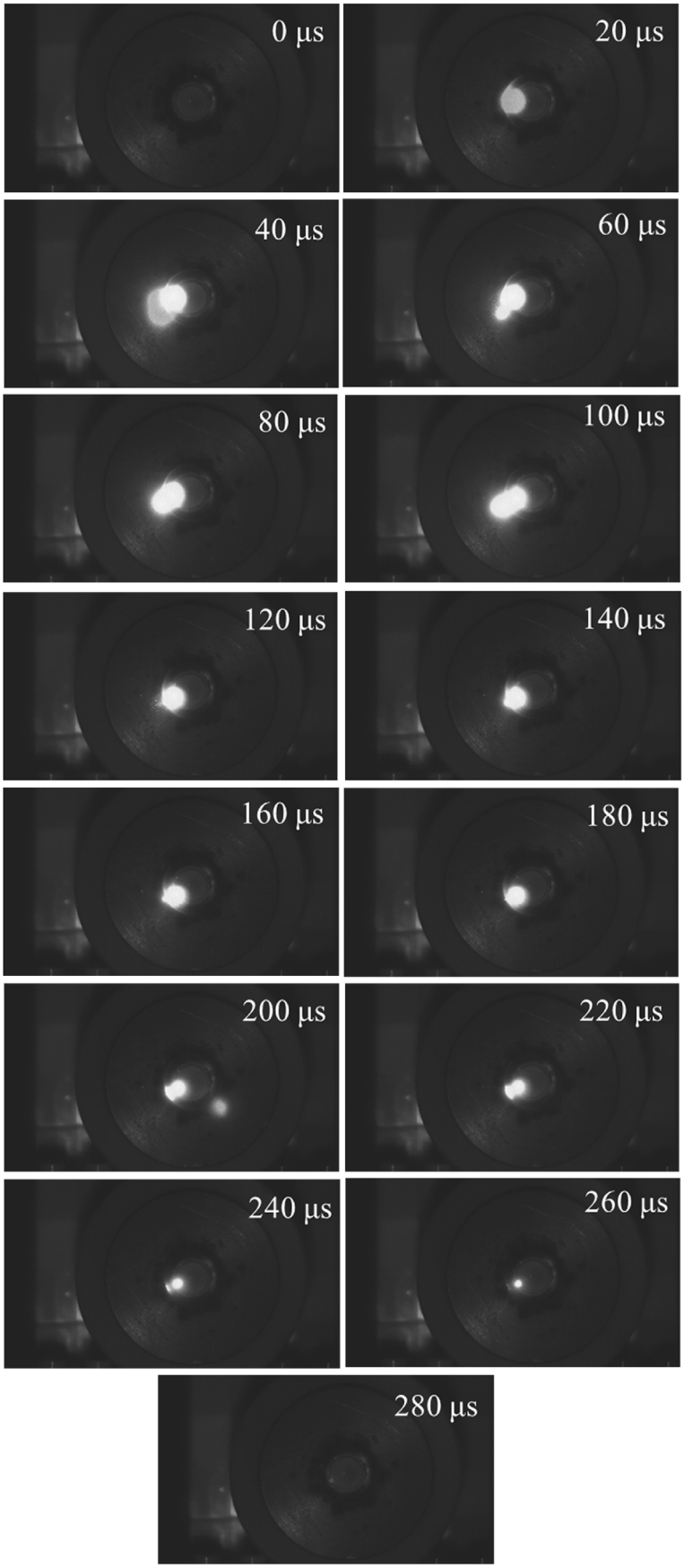

Fig. 17. High-speed camera capturing the VAT discharge images.

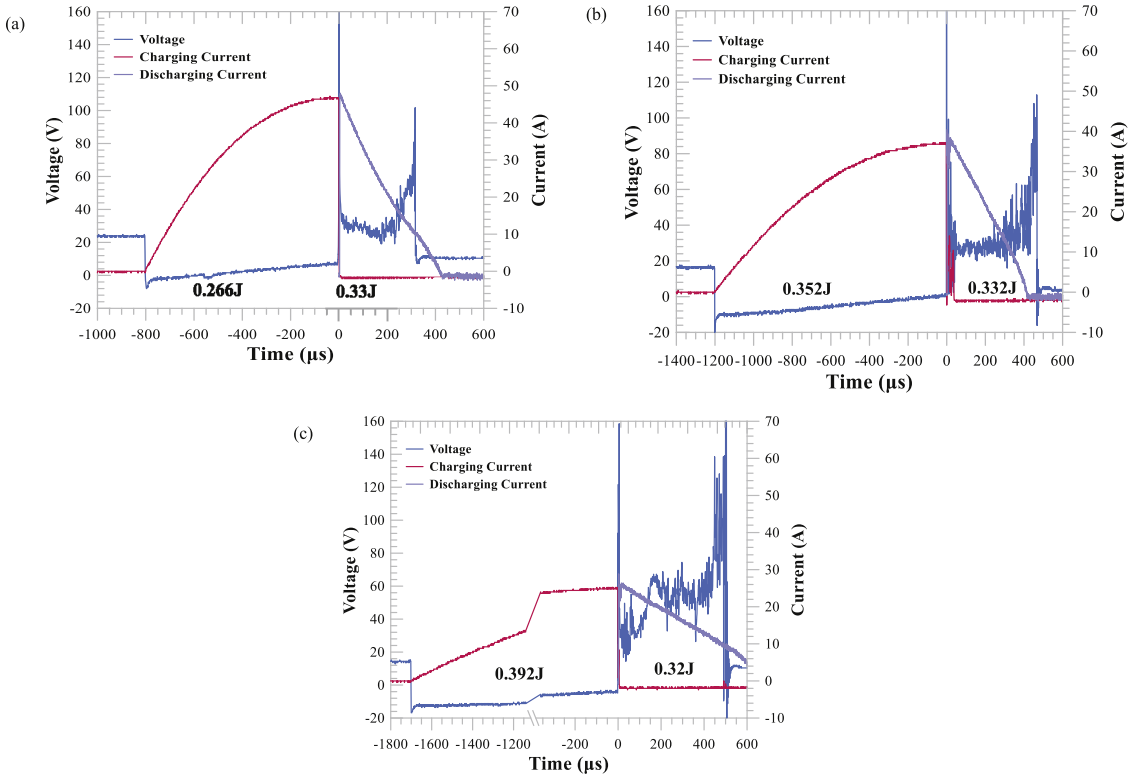

Fig. 18. Charging and discharging graphs of three different inductors: 220 μH (top), 440 μH (middle), and 1 mH (bottom).

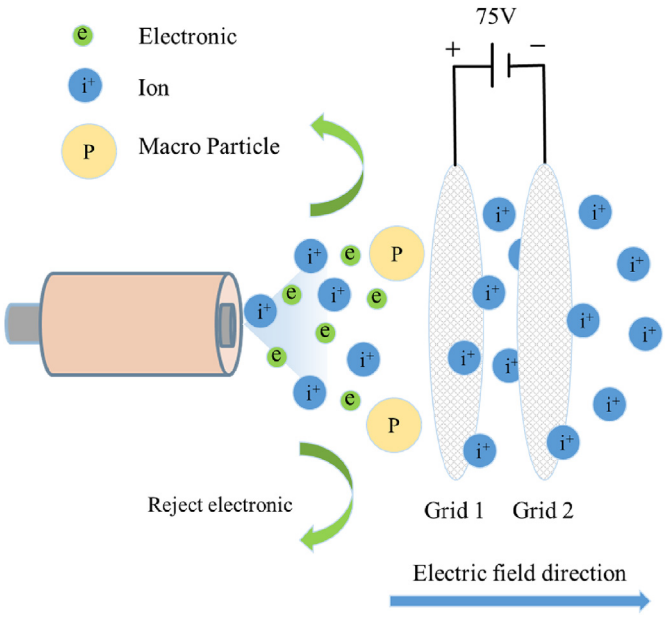

Fig. 19. Conceptual diagram of Grid measurement method.

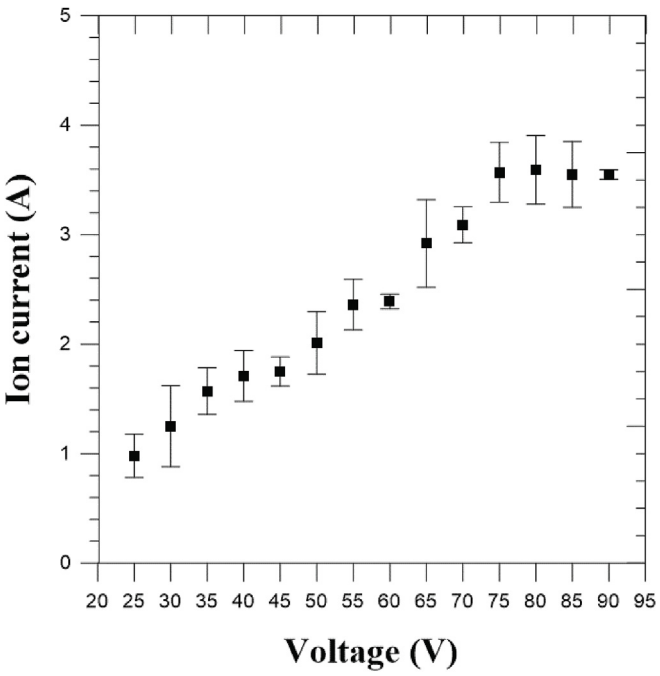

Fig. 20. Ion current and voltage relationship.

the distance between the two grids was 5 mm. By adjusting the different grid biases to measure the ion current, the relationship between current and voltage can be obtained, as shown in Fig. 20.

At low voltages, the electric field is not sufficient to exclude all electrons. Ions passing through the grid are neutralized by some of the electrons, thus causing ion current distortion. When the electric field has a bias voltage of 75 V or more, the ion current tends to be saturated. Therefore, when a bias voltage of 75 V was applied to the power grid, the maximum ion current of approximately 3.55 A was obtained. Based on the ratio of the ion current to discharge current, the ion rate was approximately 7.1%.

As the study is still in the initial stage of development, the fuel feeding system is not developed yet. Thus, the service life of the VAT without a feeding system was tested. Before evaluating life, the cathode weight was measured using an electronic balance. The change in weight was used to estimate the cathode erosion rate after the end of the experiment. The discharge frequency was set to 1 Hz under vacuum conditions of 10^{-5} hPa. The experimental results revealed that the VAT

Fig. 21. VAT surface image was taken after life test.

without a feeding system can discharge approximately 70,000 times, and the mass of ion particles by a single pulse was calculated by the following Equation (16) [17],

$$\Delta\ \mathrm{m}= \frac{f_i J_d M_i}{e} < Z^{-1}> \tag{16}$$

where f_i is ion current fraction 0.071, J_d is discharge current, M_i is the atomic mass of aluminum, e is the elementary charge, and $<Z^{-1}>$ represents the mean inverse charge state. The calculation results revealed that each discharge can issue 0.28 μg of ion particles.

Conversely, after the discharge, it was found that the metal was covered with a metal layer, as shown in Fig. 21. During the discharge process, some metal ions were recoated on the surface of the insulator to replace the carbon layer for forming a new metal conductive layer. However, when the metal ion deposition amount is higher than the amount of metal ion evaporation, the excess metal layer causes a short circuit in the VAT after a period, and the VAT life test ends. During the life test, the electrons are attracted by the anode potential and bombard the surface of the anode, thus causing contamination of the anode surface.

4.4. VAT performance analysis

To understand the performance of the VAT prototype presented in this study, a preliminary analysis of some of its performance parameters is presented in this section. Moreover, these parameters are compared with those of the VATs presented in other international studies, which is beneficial to the subsequent development and optimization of a VAT. As the VAT discharge is a pulse mode, it is usually expressed by the number of impulses that are generated using a single pulse. The common comparison parameters include impulse bit, specific impulse, thrust to power ratio, and efficiency. These parameters can be calculated based on I_{bit}, and the calculation methods for these parameters are listed separately herein. The impulse bit can be expressed using the following equation:

$$\mathrm{I_{bit}} = \Delta \mathrm{m}\vec{V}\ , \tag{17}$$

where I_{bit} is the impulse bit, Δm is the mass of ion particles, and $\vec{V}$ is the ion velocity. After calculation, the value of I_{bit} is4.31 μNs. If the thrust is changed to I_{bit}, specific impulse (I_{sp}) can be expressed as presented in Equation (17):

$$\mathrm{I_{sp}} = \frac{\mathrm{I_{bit}}}{\Delta \mathrm{mg}} \tag{18}$$

After calculation, the specific impulse value is 1571s.

The input energy is usually different in different propulsion systems. To compare the VAT performance, the ratio of thrust to power was calculated.

$$\frac{T}{P} = \frac{I_{bit}}{E}, \tag{19}$$

where E is the input energy (J) and the calculated value of T/P is 16.3 μN/W.

Efficiency (η)

Regarding VAT efficiency calculation, the output kinetic energy–input energy equation is the commonly used equation. In this study, for simplifying the problem, the conversion efficiency in the energy processing unit was neglected. Therefore, the input energy here was the energy stored in the inductor, and the equation for efficiency can be rewritten as follows:

$$\eta = \frac{\frac{1}{2}\Delta \mathrm{m}\ \vec{\mathrm{V}}^2}{\mathrm{E\ (Inductive\ stored\ energy)}} \tag{20}$$

After calculation, the efficiency of VAT is 12.5%.

The performance of the VAT proposed in this study is compared with existing VATs in Table 3 [19,30,35–38]. The VAT prototype proposed in this study is similar to that in other studies in terms of the input voltage. However, the discharge current generated by different circuit systems is different, which affects other subsequent parameters. An analysis of these parameters revealed that the performance of the VAT proposed in this study is good. However, as these values are derived using theoretical equations, in the future, an actual thrust stand is required for measuring the real-time thrust and comparing the

Table 3
Comparison between the performances of the VAT proposed in this study and that of VATs in other studies.

Paper	Parameters					
	Supply voltage (V)	Discharge current (A)	Impulse bit (μNs)	Specific impulse (s)	Thrust to power (μN/W)	Efficiency (%)
Aheieva et al. [35]	300	1000	2	1300	–	2.66
Schein et al. [36]	24.7	20	1	–	2.2	5.6
Kronhaus et al. [37]	15–35	11.5	0.11	850	4.4	1.2
Lun et al. [38]	–	< 500	0.01	2400	–	–
Schein et al. [30]	5	30	2.5	–	0.02	13
Keidar et al. [19]	5–24	100	1	1300	–	21
This study	**30**	**50**	**4.31**	**1571**	**16.3**	**12.5**

performance of various VATs. However, the current theoretical calculations can provide some preliminary outcomes for comparison.

5. Conclusions

In recent years, EP has become a major trend in the development of the space industry. As Taiwan is still in the early stage of development in this field of research, the understanding of many details of design and technologies is not yet well known. This study attempted to develop an EP system by conducting domestic independent research with the aim of laying the foundation for the development of domestic EP. Key technologies such as the trigger-less ignition mechanism and the inductor energy storage circuit design were mastered, and the preliminary performance of the VAT prototype was determined using a theoretical formula. By considering that the VAT system will be applied to microsatellites in the future, this study attempted to miniaturize the propulsion system and circuit system to facilitate integration on microsatellites. Moreover, some circuit component factors, such as heat dissipation and damage, were analyzed during circuit designing by conducting continuous testing and improvement to successfully solve the problems on the circuit. In this study, the theoretical analysis was conducted and the actual experimental parameters were measured. Under the experimental conditions of a vacuum pressure of 10^{-5} hPa, the VAT prototype with a single pulse can provide an impulse of approximately 4.31 μNs. After estimation, the specific impulse value was 1571 s, the thrust to power ratio was 16.3 μN/W, and the propulsion efficiency was approximately 12.5%. Moreover, by adjusting the different discharge frequencies, the value of the VAT output power was found to be in the range of 0.33–6.6 W. These values indicate that the VAT is suitable for space mission tasks such as attitude control and position preservation of microsatellites.

Declaration of competing interest

All authors declared that: (i) no support, financial or otherwise, has been received from any organization that may have an interest in the submitted work; and (ii) there are no other relationships or activities that could appear to have influenced the submitted work.

Acknowledgments

This work was financially supported by the Ministry of Science and Technology, Taiwan (Republic of China) under the grant numbers, MOST 105-2628-E-006-005-MY3 and MOST 108-2628-E-006-008-MY3. Furthermore, we would like to sincerely thank to Dr. Tien-Chun Kuo and Dr. Yao-Chung Hsu from National Space Organization, National Applied Research Laboratories, Taiwan (Republic of China) for granting this study.

References

[1] J. Kolbeck, J. Lukas, G. Teel, M. Keider, E. Hanlon, J. Pittman, M. Lange, J. Kang, μCAT Micro-propulsion Solution for Autonomous Mobile On-Orbit Diagnostic System, (2016).
[2] R. Goldman, W. Kerslake, W. Nieberding, SERT II-Mission, thruster performance, and in-flight thrust measurements, J. Spacecraft Rockets 8 (1971) 213–224.
[3] G. Herdrich, U. Bauder, A. Boxberger, R.A. Gabrielli, M. Lau, D. Petkow, M. Pfeiffer, C. Syring, S. Fasoulas, Advanced plasma (propulsion) concepts at IRS, Vacuum 88 (2013) 36–41.
[4] D. Bock, M. Lau, T. Schönherr, B. Wollenhaupt, G. Herdrich, H.-P. Röser, PERSEUS-In-Orbit Validation for Electric Propulsion Systems TALOS and SIMP-LEX.
[5] A.S. Pagan, C. Montag, G. Herdrich, CubeSat atmospheric probe for education (CAPE), 10 Th IAA Symposium on Small Satellitees for Earth Observation, Berlin, 2015.
[6] I.J. Jordan, Electric Propulsion: Which One for My Spacecraft, Space Systems I Course at JHU, Whiting School of Engineering, 2000.
[7] N. Qi, J. Schein, R. Binder, M. Krishnan, A. Anders, J. Polk, Compact vacuum arc micro-thruster for small satellite systems, 37th Joint Propulsion Conference and Exhibit, 2001, p. 3793.
[8] R.L. Boxman, D.M. Sanders, P.J. Martin, Handbook of Vacuum Arc Science & Technology: Fundamentals and Applications, William Andrew1996.
[9] S.R. Ramírez, D.A.S. Suárez, D.F. Devia-Narvaez, E.R. Parra, Study of the plasma behavior produced by a vacuum arc discharge for different cathode materials, DYNA: revista de la Facultad de Minas. Universidad Nacional de Colombia, Sede Medellín 85 (2018) 76–82.
[10] H.C. Miller, Electrical discharges in vacuum: 1980-90, IEEE Trans. Electr. Insul. 26 (1991) 949–1043.
[11] J. Daalder, Components of cathode erosion in vacuum arcs, J. Phys. Appl. Phys. 9 (1976) 2379.
[12] A. Gilmour, D.L. Lockwood, Pulsed metallic-plasma generators, Proc. IEEE 60 (1972) 977–991.
[13] H. Takikawa, H. Tanoue, Review of cathodic arc deposition for preparing droplet-free thin films, IEEE Trans. Plasma Sci. 35 (2007) 992–999.
[14] R. Dethlefsen, Performance measurements on a pulsed vacuum arc thruster, AIAA J. 6 (1968) 1197–1199.
[15] A.S. Gilmour, D.L. Lockwood, Pulsed metallic-plasma generators, Proc. IEEE 60 (1972) 977–991.
[16] N. Qi, J. Schein, R. Binder, M. Krishnan, A. Anders, J. Polk, Compact vacuum arc thruster for small satellite systems, IEEE Conference Record - Abstracts. PPPS-2001 Pulsed Power Plasma Science 2001. 28th IEEE International Conference on Plasma Science and 13th IEEE International Pulsed Power Conference (Cat. No.01CH37, 2001, p. 588.
[17] J.E. Polk, M.J. Sekerak, J.K. Ziemer, J. Schein, N. Qi, A. Anders, A theoretical analysis of vacuum arc thruster and vacuum arc ion thruster performance, IEEE Trans. Plasma Sci. 36 (2008) 2167–2179.
[18] P.R. Neumann, M. Bilek, D.R. McKenzie, A centre-triggered magnesium fuelled cathodic arc thruster uses sublimation to deliver a record high specific impulse, Appl. Phys. Lett. 109 (2016) 094101.
[19] M. Keidar, J. Schein, K. Wilson, A. Gerhan, M. Au, B. Tang, L. Idzkowski, M. Krishnan, I.I. Beilis, Magnetically Enhanced Vacuum Arc Thruster, MVAT), 2005.
[20] F. Rysanek, R.L. Burton, Charging of macroparticles in a pulsed vacuum arc discharge, IEEE Trans. Plasma Sci. 36 (2008) 2147–2162.
[21] S. Hohenbild, C. Grübel, G.Y. Yushkov, E.M. Oks, A. Anders, A study of vacuum arc ion velocities using a linear set of probes, J. Phys. Appl. Phys. 41 (2008) 205210.
[22] T. Zhuang, A. Shashurin, T. Denz, D. Chichka, M. Keidar, Micro-Vacuum Arc Thruster with Extended Lifetime, (2009).
[23] J. Lun, C. Law, Influence of cathode shape on vacuum arc thruster performance and operation, IEEE Trans. Plasma Sci. 43 (2015) 198–208.
[24] M. Nakamoto, K. Toyoda, S. Fuchigami, M. Cho, 300V Direct Drive Vacuum Arc Thruster for Nano-Satellite, (2013).
[25] S. Haque, C.K. Dinelli, M. Keidar, T. Lim, Quad Channel Micro-cathode Arc Thruster Electric Propulsion Subsystem for the Ballistic Reinforced Satellite, BRICSat-P), 2014.
[26] M. Pietzka, M. Kühn-Kauffeldt, J. Schein, I. Kronhaus, K. Schilling, T. Mai, A. Lebeda, Innovative vacuum arc thruster for CubeSat constellations, The 33st International Electric Propulsion Conference, The George Washington University, USA, 2013.
[27] P. Neumannn, M. Bilek, D. McKenzie, Fuel selection for pulsed cathodic Arc thrusters, J. Propul. Power 28 (2012) 218–221.
[28] M. Kandah, J.-L. Meunier, Erosion Study on Graphite Cathodes Using Pulsed Vacuum Arcs, (1996).
[29] M. Kandah, J.-L. Meunier, Vacuum Arc Cathode Spot Movement on Various Kinds of Graphite Cathodes, (1999).
[30] J. Schein, N. Qi, R. Binder, M. Krishnan, J. Ziemer, J. Polk, A. Anders, Inductive energy storage driven vacuum arc thruster, Rev. Sci. Instrum. 73 (2002) 925–927.
[31] C. Kimblin, Cathode spot erosion and ionization phenomena in the transition from vacuum to atmospheric pressure arcs, J. Appl. Phys. 45 (1974) 5235–5244.
[32] X. Zhou, J. Heberlein, An experimental investigation of factors affecting arc-cathode erosion, J. Phys. Appl. Phys. 31 (1998) 2577.
[33] M. Proschek, R. Tarrant, L. Ryves, D. McKenzie, M. Bilek, Langmuir probe measurements of drifting pulsed arc plasma, Proc. 13th Gaseous Electronics Meeting (2004) 51.
[34] D. Andruczyk, R. Tarrant, B. James, M. Bilek, G. Warr, Langmuir probe study of a titanium pulsed filtered cathodic arc discharge, Plasma Sources Sci. Technol. 15 (2006) 533.
[35] K. Aheieva, K. Toyoda, M. Cho, Vacuum Arc Thruster Development and Testing for Micro and Nano Satellites, (2016).
[36] J. Schein, N. Qi, R. Binder, M. Krishnan, J. Ziemer, J. Polk, A. Anders, Low Mass Vacuum Arc Thruster System for Station Keeping Missions, (2001).
[37] I. Kronhaus, M. Laterza, Y. Maor, Inline Screw Feeding Vacuum Arc Thruster, (2017).
[38] J. Lun, R. Dobson, W. Steyn, Performance Measurements of a Medium-Current Short-Pulsed Vacuum Arc Thruster, (2014).
[39] Yueh-Heng Li, Sunil Palagiri, Po-Yu Chang, Christoph Montag, Georg Herdrich, Plasma behavior in a solid-fed pulsed plasma thruster, Journal of Aeronautics, Astronautics and Aviation 51 (2019) 31–42, https://doi.org/10.6125/JoAAA.201903_51(1).03 In this issue.
[40] Yueh-Heng Li, Clémence Royer, Effect of voltage on second-stage electrodes of dual-stage solid propellant pulsed plasma thruster, Vacuum 167 (2019) 103–112, https://doi.org/10.1016/j.vacuum.2019.05.037 In this issue.
[41] Qimeng Xia, Ningfei Wang, Xianming Wu, Kan Xie, Song Bai, Zhang Zun, Liang Ren, The influence of external magneticfield on the plume of vacuum arc thruster, Acta Astronautica 164 (2019) 69–76, https://doi.org/10.1016/j.actaastro.2019.07.015 In this issue.